Chinese Medical Journal®

Magnesium lithospermate B enhances the potential of human-induced pluripotent stem cell-derived cardiomyocytes for myocardial repair

Chengming Fan[1,2,3], Kele Qin[1], Chukwuemeka Daniel Iroegbu[1], Kun Xiang[1], Yibo Gong[1], Qing Guan[1], Wenxiang Wang[4], Jun Peng[2], Jianjun Guo[3], Xun Wu[1,4], Jinfu Yang[1]

[1]Department of Cardiovascular Surgery, The Second Xiangya Hospital, Central South University, Changsha, Hunan 410011, China;
[2]Department of Pharmacology, Xiangya School of Pharmaceutical Sciences, Central South University, Changsha, Hunan 410078, China;
[3]Hunan Fangsheng Pharmaceutical Co., Ltd., Changsha, Hunan 410000, China;
[4]Department of Thoracic Surgery, The Affiliated Cancer Hospital of Xiangya School of Medicine, Central South University, Changsha, Hunan 41000, China.

Abstract

Background: We previously reported that activation of the cell cycle in human-induced pluripotent stem cell-derived cardiomyocytes (hiPSC-CMs) enhances their remuscularization capacity after human cardiac muscle patch transplantation in infarcted mouse hearts. Herein, we sought to identify the effect of magnesium lithospermate B (MLB) on hiPSC-CMs during myocardial repair using a myocardial infarction (MI) mouse model.

Methods: In C57BL/6 mice, MI was surgically induced by ligating the left anterior descending coronary artery. The mice were randomly divided into five groups (n = 10 per group); a MI group (treated with phosphate-buffered saline only), a hiPSC-CMs group, a MLB group, a hiPSC-CMs + MLB group, and a Sham operation group. Cardiac function and MLB therapeutic efficacy were evaluated by echocardiography and histochemical staining 4 weeks after surgery. To identify the associated mechanism, nuclear factor (NF)-κB p65 and intercellular cell adhesion molecule-1 (ICAM1) signals, cell adhesion ability, generation of reactive oxygen species, and rates of apoptosis were detected in human umbilical vein endothelial cells (HUVECs) and hiPSC-CMs.

Results: After 4 weeks of transplantation, the number of cells that engrafted in the hiPSC-CMs + MLB group was about five times higher than those in the hiPSC-CMs group. Additionally, MLB treatment significantly reduced tohoku hospital pediatrics-1 (THP-1) cell adhesion, ICAM1 expression, NF-κB nuclear translocation, reactive oxygen species production, NF-κB p65 phosphorylation, and cell apoptosis in HUVECs cultured under hypoxia. Similarly, treatment with MLB significantly inhibited the apoptosis of hiPSC-CMs *via* enhancing signal transducer and activator of transcription 3 (STAT3) phosphorylation and B-cell lymphoma-2 (BCL2) expression, promoting STAT3 nuclear translocation, and downregulating BCL2-Associated X, dual specificity phosphatase 2 (DUSP2), and cleaved-caspase-3 expression under hypoxia. Furthermore, MLB significantly suppressed the production of malondialdehyde and lactate dehydrogenase and the reduction in glutathione content induced by hypoxia in both HUVECs and hiPSC-CMs *in vitro*.

Conclusions: MLB significantly enhanced the potential of hiPSC-CMs in repairing injured myocardium by improving endothelial cell function *via* the NF-κB/ICAM1 pathway and inhibiting hiPSC-CMs apoptosis *via* the DUSP2/STAT3 pathway.

Keywords: Myocardial infarction; Cell therapy; Induced pluripotent stem cells; Magnesium lithospermate B; Cardiomyocyte; Disease modeling; hiPSC-CMs

Introduction

Ischemic heart disease, resulting from coronary obstruction, accounts for 80% of deaths from cardiovascular disease (CVD).[1] We previously reported that the activation of the cell cycle in human-induced pluripotent stem cell-derived cardiomyocytes (hiPSC-CMs) *via* chemical exposure or genetic modification enhances their remuscularization capacity after transplantation into the infarcted mouse heart.[2–4] However, restricted engraftment ability and the inflammatory microenvironment are major barriers to conventional cardiac cell therapies, including transplantation.[5–7] The infiltration of inflammatory cells results in the secretion of proteolytic enzymes and reactive oxygen species (ROS), which increases the damage at the infarct site.[8] Accordingly, ischemic heart disease therapy that focuses on suppressing the body's hyperactive inflam-

Access this article online

Quick Response Code:

Website: www.cmj.org

DOI: 10.1097/CM9.0000000000002867

Correspondence to: Jinfu Yang, Department of Cardiovascular Surgery, The Second Xiangya Hospital, Central South University, Changsha, Hunan 410011, China
E-Mail: yjf19682005@csu.edu.cn;
Xun Wu, Department of Cardiovascular Surgery, The Second Xiangya Hospital, Central South University, Changsha, Hunan 410011, China
E-Mail: xuwu9010@163.com

Chinese Medical Journal 2024;137(15)

Received: 22-08-2023; **Online:** 15-01-2024 **Edited by:** Sihan Zhou and Xiuyuan Hao

matory response is regarded as a feasible scheme.[9] *Salvia miltiorrhiza* is a widely used traditional Chinese medicine for treating hyperviscosity and blood stasis.[10] The primary water-soluble bioactive component of *Salvia miltiorrhiza*, magnesium lithospermate B (MLB), has shown promising effect in preventing and treating cardiovascular damage in recent research being employed in *in vivo* and *in vitro* models.[11] MLB exhibits various pharmacological activities, such as antioxidant and anti-fibrotic effects.[12–14] Additionally, MLB can counteract lipopolysaccharide (LPS)-induced neuroinflammatory responses in BV2 microglia and inhibit the inflammatory response by suppressing nuclear factor (NF)-κB activation in activated T cells.[15]

However, little is known about MLB's effect on hiPSC-CMs during myocardial repair. This research sought to explore whether MLB could improve endothelial cell function after myocardial infarction (MI), suppress inflammatory response at the infarcted area, and inhibit the apoptosis of transplanted hiPSC-CMs, thereby improving the survival rate of hiPSC-CMs and, consequently enhancing cardiac function.

Methods

hiPSC-CMs, HUVECs, and THP-1 cell culture

Nanjing Help Stem Cell Innovations Co., Ltd. provided the hiPSC-CMs, cardiomyocyte digestion media, and cardiomyocyte maintain medium used in this study. HiPSC-CMs were cultured on Petri dishes coated with cardiomyocyte plating medium and used after 60 days of maturation and stabilization following differentiation. In addition, 10% fetal bovine serum (FBS), 0.05 mg/mL endothelial cell culture supplement, and 1% penicillin/streptomycin were added to the endothelial cell medium used to culture the human umbilical vein endothelial cells (HUVECs) (ScienCell Research Laboratories, San Diego, CA, USA). Subsequently, β-mercaptoethanol (0.05 mmol/L) and 10% FBS were added to Roswell Park Memorial Institute (RPMI) 1640 medium to culture THP-1 cells (ATCC, Manzas, Virginia, USA, TIB-202).

Establishment of a mouse model of acute MI and intramyocardial stem cell injection

The Ethics Committee of Central South University's Second Xiangya Hospital approved all animal studies before they were conducted (No. 2021046). C57BL/6 mice (Hunan SJA Laboratory Animal Co., Ltd, Hunan, China) were kept in a controlled environment with a 12-h light/12-h dark cycle at 25°C temperature with 40–60% humidity, and acute MI was surgically induced after 8 weeks. Briefly, mice were randomized into 5 groups (10 mice per group) and received isoflurane (1.5–2.0%; VetOne, Boise, Idaho, USA) inhalation anesthesia, intubation, and artificial ventilation. Then, non-absorbable 8-0 suture was used to ligate the left anterior descending (LAD) coronary artery during a left thoracotomy. A total of 3×10^5 hiPSC-CMs (1×10^5 cells per point) were injected at two points to border the infarct zone and at one point in the central area of the infarct site with (hiPSC-CMs + MLB group) or without (hiPSC-CMs group) intraperitoneally delivery of MLB ($15\ mg \cdot kg^{-1} \cdot d^{-1}$, Green Valley Pharmaceuticals, Shanghai, China) for 7 days after the operation. Mice in the MLB group received MLB as above but no hiPSC-CMs. In the Sham group, a suture was wound around the LAD coronary artery but no ligation was performed. Finally, the mice with MI not subjected to MLB or hiPSC-CM injection were set as the MI group [Supplementary Table 1, http://links.lww.com/CM9/B750]. All the animals received an intraperitoneal injection of buprenorphine (0.1 mg/kg for 3 days), carprofen (5 mg/kg for 1 day), and cyclosporine A (10 mg/kg for 30 days) every 12 h. Seven days post-surgery, heart sections were obtained from five mice from each group for histological analysis. No death events were reported from peri-/post-operative complications.

Echocardiography

Echocardiographic imaging of mice before and 4 weeks after inducing MI was performed, as previously described. Briefly, anesthesia was induced with 1.5–2.0% isoflurane and maintained till the animals' heart rates stabilized at 400–500 beats per minute. High-resolution micro-ultrasound equipment (Vevo 2100, VisualSonics, Inc., Toronto, Canada) was used to obtain B-mode and two-dimensional M-mode images from long- and short-axis views, respectively. Lastly, in a short-axis view (at the level of the papillary muscles), vevo analytic software (Vevo 2100, VisualSonics, Inc., Toronto, Canada) was used to compute the left ventricular ejection fraction (LVEF) and the left ventricular fractional shortening (LVFS). The identification of the experimental group was blinded for the operator.

Immunostaining

Following surgery, the hearts of mice belonging to various treatment groups were extracted on days 7 and 28 after the procedure and processed, as previously described.[2,4] Briefly, ice-cold 4% paraformaldehyde (PFA) was used to fix the cardiac tissue for 4 h before soaking them overnight in 30% sucrose. After permeabilization with 0.2% Triton X-100 for 10 min at room temperature (RT), serial 10-micron cryosections were then blocked for half an hour at RT using 5% donkey serum in Dulbecco's phosphate-buffered saline (DPBS, pH: 7.4). This was followed by incubation of the samples for 16 h at 4°C with primary antibodies (diluted 1:10 to 1:10,000 in blocking buffer [1.5% bovine serum albumin, 100 mmol/L glycine in PBS]), and then with secondary antibodies (1:200 dilutions) at RT in a dark environment for 2 h in a blocking buffer. Counterstaining with 4′, 6-dimethyl-2-phenyl-indole (DAPI, 1.5 μg/mL; Vector Laboratories, Newark, CA, USA) was performed on the nuclei. Secondary antibody-only staining was performed to serve as the negative control. Antibodies targeting CD31 (ab24590), BCL2 (ab182858), CD11b

(ab133357), cardiac troponin T (cTnT) (ab91605), cardiac troponin (cTnI) (ab47003), and α-actinin (ab9465); Alexa Fluor 555-conjugated donkey anti-rabbit IgG (H&L) (ab150074); Alexa Fluor 488-conjugated donkey anti-mouse IgG (H&L) (ab150105); and calcein Acetoxymethyl (ab141420) were procured from Abcam (Cambridge, UK). Antibodies against F4/80 (#70076), cleaved-caspase-3 (9664s), p-inhibitor of kB (IκB)α (# 2859), STAT3 (126405), p-IkB kinase (IKK)α/β (#2697), p-STAT3 (9145s), phosphorylated (p)-NF-κB p65 (3033S), and NF-κB p65 (8242S) were supplied by Cell Signaling Technology (Danvers, MA, USA). Griffonia Simplicifolia Lectin I (GSL I) Isolectin B4, Fluorescein (FL-1201-0.5) was purchased from Vector Laboratories. Lastly, the sections were analyzed and imaged with the aid of a fluorescence microscope.

Immunohistochemical (IHC) staining

Xylene was used to deparaffinize slices of hearts obtained on days 7 and 28 post-surgery for 2 × 20 min before rehydration in ethanol (100%, 95%, 85%, and 75%, 5 min each stage). Antigen retrieval consisted of immersing the slices in 0.01 mol/L citrate buffer (pH 6.0) with distilled water for 5 min, boiling them in an electric furnace or microwave oven, cooking them continuously for 15 min, and then allowing them to cool to RT. After washing three times in 0.01 mol/L PBS (pH 7.2–7.6), 3 min each wash, the slices were immersed in 3% H_2O_2 for 10 min at RT to inactivate endogenous peroxidases and then rinsed thrice using PBS, 3 min each time. Following overnight incubation at 4°C using primary antibodies against CD11b (ab133357, Abcam, Cambridge, UK) and F4/80 (# 70076, Cell Signaling Technology, Danvers, MA, USA), the slices were washed thrice for 5 min each time in PBS, after which a secondary antibody (HRP-conjugated anti-rabbit IgG antibody; 50–100 μL added dropwise) was used to incubate the samples at 37°C for half an hour. DAB working solution (50–100 μL) was introduced dropwise after samples were rinsed in PBS (3 × 5 min), and the samples were subjected to incubation for 1.5 min until color development (detected under a microscope). Thereafter, distilled water was used to wash the sections before counterstaining them with hematoxylin for 5–10 min, rinsing them with distilled water, returning them to blue with PBS, and dehydrating them in a graded alcohol series (60–100%, 5 min each step). After being placed in xylene twice for 10 min each, the samples were sealed using neutral gum, examined under a microscope, and photographed.

Cell viability assay

The viability of cells was characterized utilizing a cell counting kit-8 (CCK-8, Yeasen Biotech Co., Shanghai, China), which was used as directed by the manufacturer. Succinctly, 96-well plates were used to seed cells (3×10^5 cells/mL) for 12 h, followed by incubation with different concentrations of MLB (0–120 μmol/L) for 24 h. Following the addition of CCK-8 reagent (10 μL) to each well, the cells were subjected to incubation for 4 h at 37°C. At last, the absorbance per well was measured by using a microplate reader (BioTek, USA) at 450 nm.

Measurement of oxidative stress

The levels of ROS, glutathione disulfide (GSSG), malondialdehyde (MDA), glutathione (GSH), lactate dehydrogenase (LDH) were evaluated utilizing respective assay kits (Jiangsu Beyotime, China) as directed by the manufacturer.

Monocyte adhesion assay

In 24-well plates HUVECs were seeded at a density of 2×10^2 cells/mL and then processed as previously indicated.[4] For half an hour at 37°C in a dark environment, THP-1 cells (ScienCell Research Laboratories, San Diego, CA, USA) were labeled with 5 μmol/L 2′-7′-bis (carboxyethyl) -5(6) -carboxyfluorescein acetoxymethyl ester diluted in RPMI 1640 medium. After removing the HUVECs medium, labeled THP-1 cells (5×10^5/mL) were then introduced to the HUVECs and subjected to incubation for 1 h at 37°C. After washing with PBS to remove non-adherent cells, adhered THP-1 cells were imaged *via* fluorescence microscopy and quantified.

Transient transfection with small interfering RNA (siRNA)

Endogenous STAT3, DUSP2, and NF-κB in HUVECs and hiPSC-CMs were knocked down by adding 100 nmol/L of Lipofectamine RNAiMAX (Invitrogen, Carlsbad, CA, USA) to the respective culture media. The next steps involved the aspiration of the previous culture media, three washes in PBS, and incubation in a culture medium containing Lipofectamine, without antibiotics, for 24 h under corresponding conditions as directed by the manufacturer. The primer sequences used can be seen in [Supplementary file, http://links.lww.com/CM9/B750].

RNA production and quantitative reverse transcription-polymerase chain reaction (qRT-PCR)

After isolating cellular total RNA, cDNA was generated by reverse transcription utilizing a GoScript kit (Promega, Madison, Wisconsin USA), as instructed by the manufacturer. After being collected, cDNA was employed as a template for qPCR, which was conducted with SYBR green on an ABI Prism 7900 Sequence Detection System as directed by the manufacturer. The internal control used was GAPDH. PCR primers can be seen in [Supplementary file, http://links.lww.com/CM9/B750].

Western blot assay

A BCA protein kit (Solarbio Life Sciences, Beijing, China) was utilized to quantify the protein concentration following the manufacturer's instructions. After denaturation at 100°C for 5 min, 2 × sample buffer was added, the protein was separated by sodium dodecyl-sulfate polyacrylamide gel electrophoresis (25 μg/pore) at constant voltage (120 V) and then transferred to polyvinylidene fluoride (PVDF) membranes (Trans-Blot

Turbo Mini PVDF Transfer Packs, Bio-Rad, USA) at 120 V for about 2 h. A blocking buffer (5% non-fat dry milk in 25 mmol/L Tris-buffered saline [TBS]) was used to block the membranes for 2 h after which they were subjected to incubation at 4°C overnight with primary antibodies. This was followed by three washes in TBS with Tween (TBST, for 10–15 min each), one-hour incubation with HRP-conjugated secondary antibody (1: 10,000 dilution) at RT, and another wash in TBST. Finally, bands were detected using the ECL reagent. Densitometric analysis was performed using AlphaVIEW SA software v.3.4 (Informer Technologies, Inc., Los Angeles, CA, USA).

Terminal deoxynucleotidyl transferase dUTP nick-end labeling (TUNEL) assay for detecting apoptotic cells

Applying fluorescent microscopy, apoptosis was detected and quantified at the single-cell level utilizing the *In Situ* Cell Death Detection Kit (Roche, Basel, Switzerland). Succinctly, samples were collected at defined time points, cryosectioned, rinsed twice in DPBS (pH 7.4), fixed in 4% PFA for 20 min at RT, and labeled with the TUNEL reaction mixture following the manufacturer's instructions. Finally, a DAPI-containing mounting medium (1.5 μg/mL; Vector Laboratories) was used to mount the samples, after which they were observed and imaged under a microscope.

Quantification of transplanted hiPSC-CMs

Frozen sections of cardiac tissues were subjected to histoimmunofluorescence staining for human-specific nuclear antigen (HNA) and non-specific sarcomeric alpha-actinin or cTnT. Transplanted hiPSC-CMs were quantified, as previously described.[5] Briefly, following the serial sectioning of the whole heart, one section out of every 50 was chosen to be stained with fluorescence. Randomly selected high-magnification images at a scale of five were taken from each section. The number of transplanted cells in each image was calculated and set as An/μm^2; the total area of each section was calculated and set as Bn/μm^2; and the number of transplanted cells in each slice was calculated as An × Bn. Accordingly, the number of transplanted cells per mouse heart = (A1 × B1 + A2 × B2 + ⋯ + An × Bn) × 50.

Assessment of MI size

Isolated mouse hearts were frozen and cut cross-sectionally (along the short axis) into 10-μm thick slices from the apex to the base. One in every 30 slices was fixed in pre-warmed Bouin's solution at 58°C , rinsed with distilled water until the yellow Bouin's solution on the slides had been completely removed, soaked in 0.1% Fast Green staining solution for 10 min at 58°C, placed directly in 1% glacial acetic acid for 2 min, rinsed once with distilled water, allowed to dry, incubated in 0.1% sirius red dye for 10 min at RT, and dehydrated using a graded alcohol series (70% alcohol for 1 min, 90% alcohol for 1 min, 100% alcohol for 1 min). Finally, the neutral resin was dripped onto the tissue, which was then cover-slipped. The normal myocardium of the heart was stained green, whereas the scar tissue was stained red. After taking complete cross-sectional images of the heart underneath the microscope, we utilized ImageJ software (Bethesda, Maryland, USA) to analyze them. The below formula was used to compute the MI area: MI area = (the sum of the length of the scar curve from the apex to the base of the heart × 30)/(the sum of the length of the left ventricle from the apex to the base of the heart × 30) × 100%.

Statistical analysis

The SPSS Institute-developed Statistical Products and Services Solutions v. 21.0 (Chicago, IL, USA) program was utilized to analyze all data, which were expressed as mean ± standard error. To analyze the variations between the two groups, an independent samples *t*-test was used. When comparing variations among three or more groups, one-way analysis of variance with Dunn's multiple comparisons test was utilized. *P* values <0.05 indicated the significance threshold. For *in vivo* study, five repeated animals were performed and for *in vitro* study three repetitions were conducted.

Results

HiPSC-CMs + MLB treatment improved cardiac function in a murine model of MI

Echocardiography was used to evaluate left ventricular functioning before MI induction (baseline, pre-op) and 28 days after the operation (post-op) [Figure 1A]. The LVEF of the MI group was considerably reduced in contrast with that of the sham-operated group (from 70% to 30%). Meanwhile, as opposed to the MI group, the LVEF and LVFS were substantially elevated in both hiPSC-CM groups, with a more prominent increase in hiPSC-CMs + MLB treated mice [Figure 1B, C]. Similarly, the end-systolic dimension (ESD) and the end-diastolic dimension (EDD) of hiPSC-CMs + MLB treated hearts were significantly reduced compared to those of other treatment groups [Figure 1D, E].

HiPSC-CMs + MLB treatment reduced myocardial infarct size and enhanced hiPSC-CMs' survival rate in mice

We further assessed the infarct size and hiPSC-CM survival in mice with MI [Figure 2]. At 28 days after MI induction, sirius red/fast green staining illustrated that the infarct size in the MLB, hiPSC-CM, and hiPSC-CMs + MLB groups was significantly decreased relative to that in the MI group, and was remarkably reduced (approximately 30%) in the hiPSC-CMs + MLB group as opposed to the MLB or hiPSC-CMs groups [Figure 2C]. The collagen volume fraction in hiPSC-CMs + MLB treated mice was reduced by 45% relative to that in MI mice; however, in the hiPSC-CMs group, the collagen volume fraction was only reduced by 13% in contrast with that of animals in the MI group [Figure 2D]. Left ventricular free wall thickness in the hiPSC-CMs + MLB and hiPSC-CMs groups was around 1.8- and 1.4-fold greater than in the MI group, correspondingly [Figure 2E].

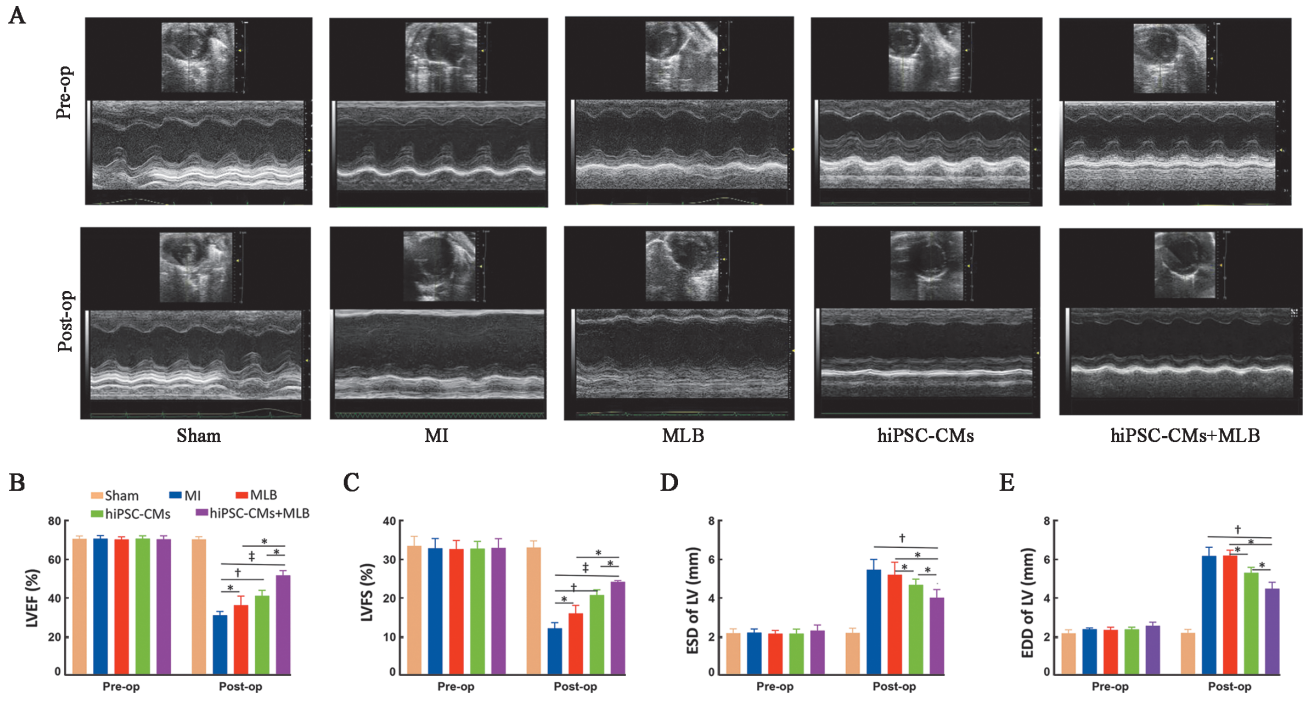

Figure 1: HiPSC-CMs + MLB treatment improved cardiac function in mice after the induction of myocardial infarction. Left ventricular function was assessed using high-resolution echocardiography (A) before (pre-op) and 4 weeks after (post-op) MI induction. LVEF (B), LVFS (C), end-systolic diameter (D), and end-diastolic diameter (E) were measured ($n = 5$; $^{*}P < 0.05$, $^{\dagger}P < 0.01$, $^{\ddagger}P < 0.001$). EDD: End-diastolic dimension; ESD: End-systolic dimension; hiPSC-CMs: Human-induced pluripotent stem cell-derived cardiomyocytes; LV: Left ventricular; LVEF: Left ventricular ejection fraction; LVFS: Left ventricular fractional shortening; MI: Myocardial infarction; MLB: Magnesium lithospermate B.

The transplanted hiPSC-CMs could be detected in the core of the infarct site as well as in peri-infarct areas of hearts from both the hiPSC-CMs and hiPSC-CMs + MLB groups 28 days after the operation [Figure 2B]. The number of grafted cells in the hearts of hiPSC-CMs + MLB treated mice was significantly higher (approximately 5-fold) than that in the hearts of the hiPSC-CMs treated mice [Figure 2F].

HiPSC-CMs + MLB treatment enhanced angiogenesis and alleviated myocardial hypertrophy in the peri-infarct zone of mice with MI

Immunostaining for the endothelium marker isolectin B4 (IB4) was conducted to assess neo-angiogenesis in the peri-infarct border regions [Figure 3A]. The vessel and arterial densities were significantly higher in the MLB, hiPSC-CMs, and hiPSC-CMs + MLB groups than in the MI group on day 28 post-surgery. Notably, vessel and arterial densities were approximately twofold greater in hiPSC-CMs + MLB-treated mice relative to the hiPSC-CMs group [Figure 3A]. We further assessed the extent to which the hearts of mice in each group exhibited cardiomyocyte hypertrophy by measuring the minimum fiber diameter (MFD) through the fluorescence staining of cell membranes with wheat germ agglutinin (WGA) in the infarct border zone and cTnT fluorescence staining in the cytoplasm of cardiomyocytes [Figure 3B]. The data showed that the MFD was substantially elevated in all the MI groups in comparison with the Sham group. Among the MI model groups, the MFD was considerably reduced in the MLB, hiPSC-CMs, and hiPSC-CMs + MLB groups relative to the MI group, with the hiPSC-CMs + MLB-treated mice displaying the smallest value [Figure 3B].

HiPSC-CMs + MLB treatment led to a significant reduction in myocardial cell apoptosis, inflammatory cell infiltration, and ICAM1 expression in the myocardial peri-infarct zone in MI model mice

We further evaluated myocardial cell apoptosis in the myocardial peri-infarct region of mice 28 days post-MI induction [Figure 4A, B]. TUNEL and cTnT staining results illustrated that the number of apoptotic cardiomyocytes was considerably elevated in all four MI groups relative to the sham-operated animals. Furthermore, the cellular apoptotic level was remarkably increased in the MI group as opposed to that in the MLB, hiPSC-CMs, and hiPSC-CMs + MLB groups, with hiPSC-CMs + MLB-treated mice exhibiting the lowest levels [Figure 4B]. Next, we assessed the extent of inflammatory cell infiltration and ICAM1 expression levels in heart sections obtained 1 week after the operation *via* immunofluorescence and IHC staining. As opposed to the MI group, the ICAM1 expression in CD31-positive endothelial cells was remarkably decreased in the MLB, hiPSC-CMs, and hiPSC-CMs + MLB groups [Figure 4C]. Similarly, the numbers of CD11b-positive myeloid cells and F4/80-positive macrophages in the myocardium of mice in the MLB, hiPSC-CMs, and hiPSC-CMs + MLB groups were considerably reduced relative to those of animals in the MI group, and these effects were most pronounced in hiPSC-CMs + MLB-treated mice [Figure 4D–G].

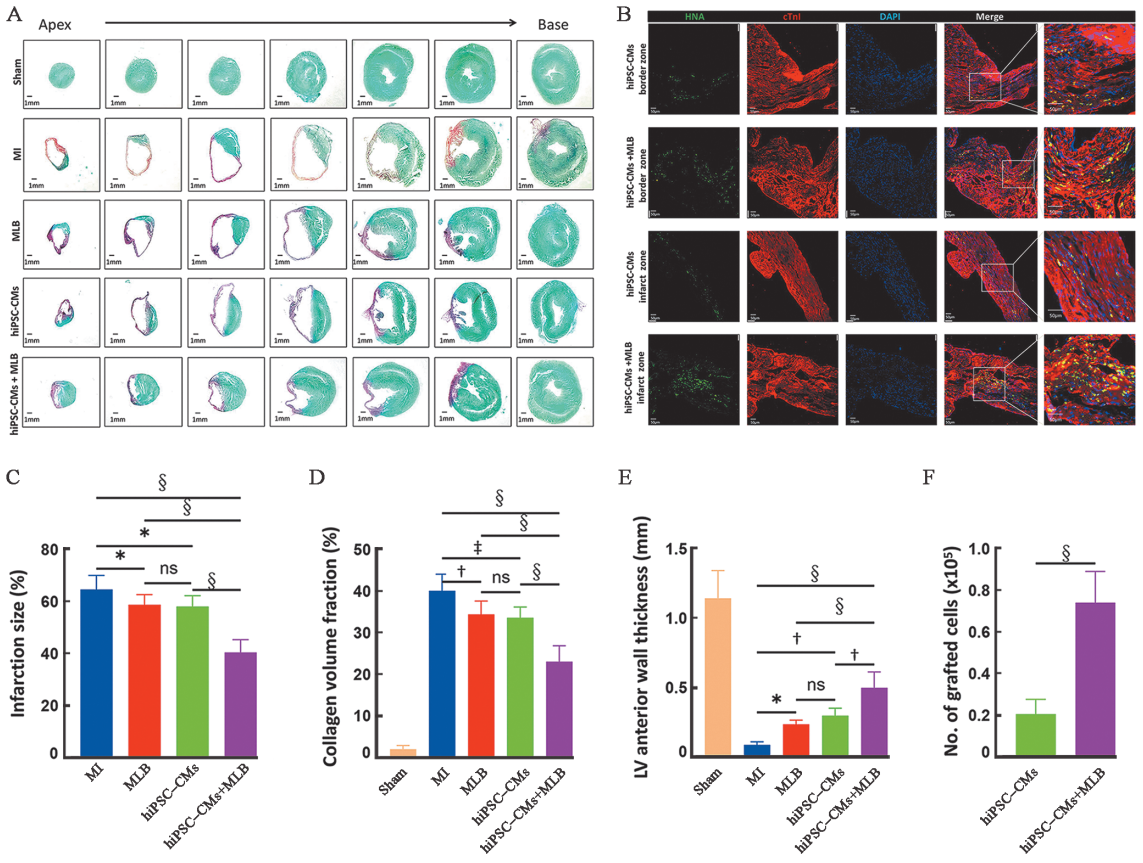

Figure 2: HiPSC-CMs + MLB treatment reduced myocardial infarct size and enhanced the survival of transplanted hiPSC-CMs. Cardiac tissue was obtained from each group at 4 weeks post-surgery and serially sectioned from the myocardium to the apex of the heart. The fibrotic (red) and non-fibrotic (green) areas of the ventricular tissue sections were stained with sirius red/fast green (A) to quantify the size of the myocardial infarct area. Grafted hiPSC-CMs (B) were also detected *via* HNA (green), cTn I (red), and DAPI (blue) staining. The infarct size (C), the fraction of collagen volume (D), and the thickness of the anterior wall of the left ventricle (E) were measured. Grafted cells were defined as those expressing HNA and counted (F) ($n = 5$; $^{*}P < 0.05$, $^{\dagger}P < 0.01$, $^{\ddagger}P < 0.001$, $^{\S}P < 0.0001$). cTnI: Cardiac troponin I; hiPSC-CMs: Human-induced pluripotent stem cell-derived cardiomyocytes; HNA: Human-specific nuclear antigen; MI: Myocardial infarction; MLB: Magnesium lithospermate B; LV: Left ventricular; ns: No statistical difference; No.: Number.

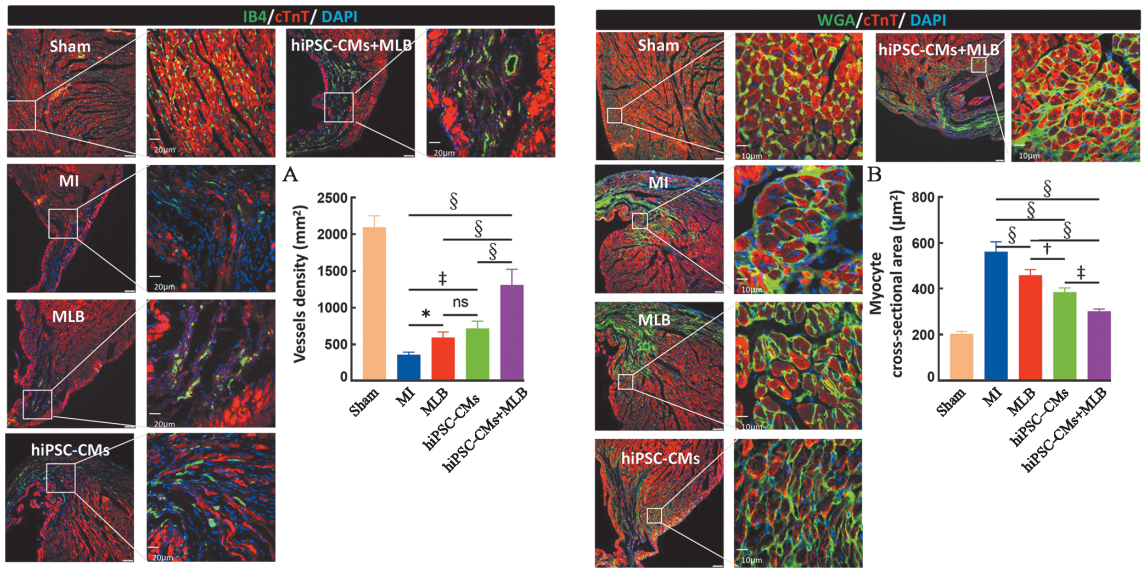

Figure 3: HiPSC-CMs + MLB treatment enhanced neovascularization and alleviated myocardial hypertrophy in the infarct border zone of mice with myocardial infarction. Assessment of angiogenesis (A) and myocardial hypertrophy (B) in the MI marginal area. IB4 (green) was used to stain vascular endothelial cells while cTnT (red) was used to stain cardiac myocytes; nuclei were counterstained with DAPI (blue). The number of capillaries was quantified as the number of IB4-positive vascular structures per square millimeter of the peri-infarct area (A). Absolute values were derived from the results of measurements taken on the cardiomyocytes' cross-sectional areas (B) ($n = 5$; $^{*}P < 0.05$, $^{\dagger}P < 0.01$, $^{\ddagger}P < 0.001$, $^{\S}P < 0.0001$). cTnT: Cardiac troponin T; hiPSC-CMs: Human-induced pluripotent stem cell-derived cardiomyocytes; MI: Myocardial infarction; MLB: Magnesium lithospermate B.

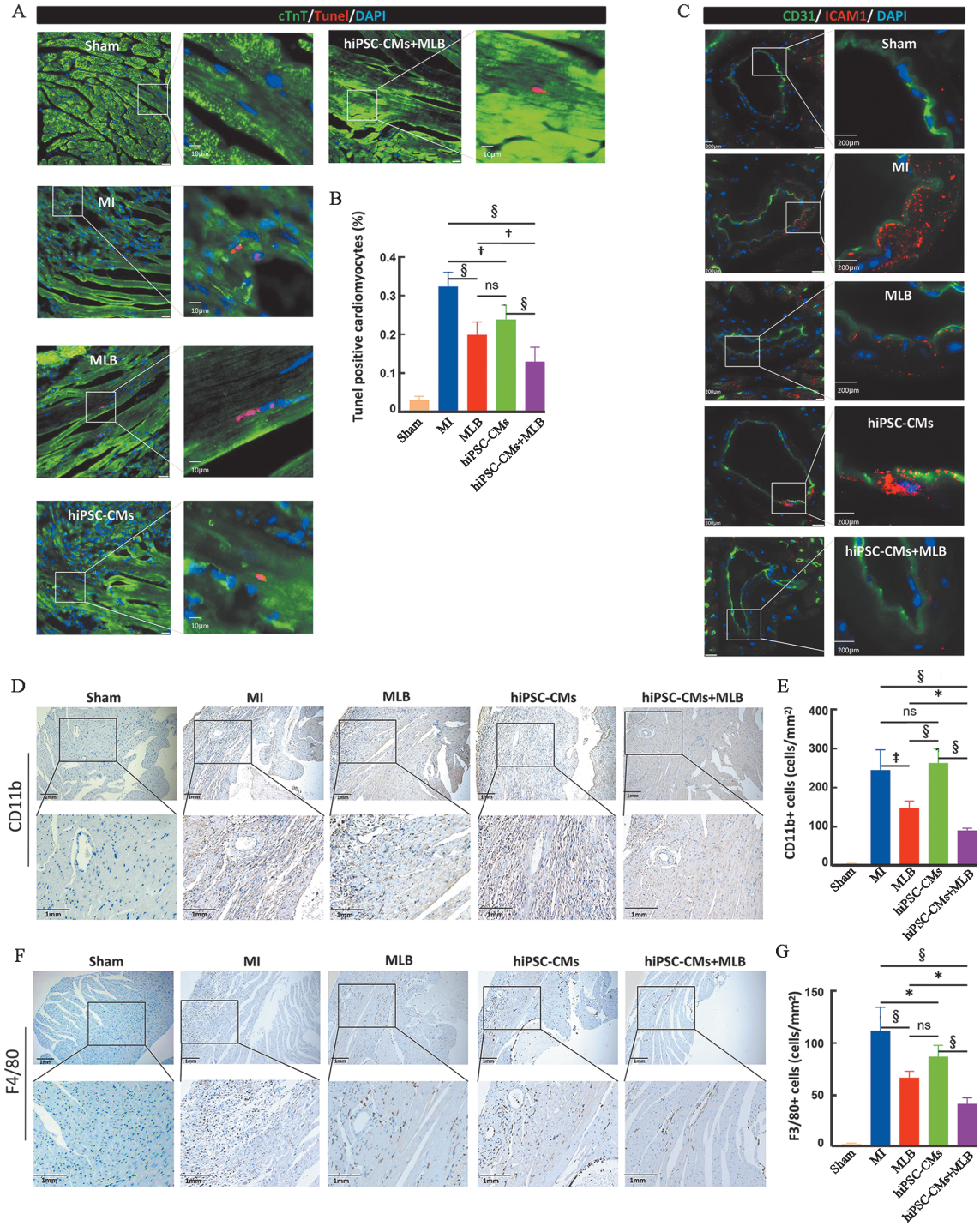

Figure 4: HiPSC-CMs + MLB treatment significantly reduced cardiomyocyte apoptosis, ICAM1 expression, and inflammatory cell infiltration in the infarct border zone in mice with myocardial infarction. One week post-surgery, heart sections were fluorescently stained for TUNEL (red) and cTnT (green) to label apoptotic cardiomyocytes (A). The proportion of TUNEL-positive cells among all cells was calculated and expressed as a percentage (B). Vascular endothelial cells were stained with CD31 (green), ICAM1 is shown in red (C), and nuclei were labeled with DAPI (blue). IHC staining for CD11b-positive neutrophils (D) and F4/80-positive macrophages (F) in the hearts of mice from the five groups. The data are presented as CD11b-positive (E) or F4/80-positive (G) cells per square millimeter ($n = 5$; $^{*}P < 0.05$, $^{\dagger}P < 0.01$, $^{\ddagger}P < 0.001$, $^{\S}P < 0.0001$). cTnT: Cardiac troponin T; hiPSC-CMs: Human-induced pluripotent stem cell-derived cardiomyocytes; IHC: Immunohistochemical; MLB: Magnesium lithospermate B.

Effects of MLB on NF-κB p65 and ICAM1 signaling in HUVECs

The mechanisms underlying the effects of MLB were investigated using an *in vitro* cell culture system. HUVECs were exposed to varying dosages of MLB (0, 10, 20, 40, 80, and 120 mmol/L), after which the CCK-8 test was conducted to determine cell viability. We discovered that under normoxia, 120 μmol/L MLB significantly inhibited the viability of HUVECs after 24 h of incubation [Figure 5A]. Next, we treated HUVECs with different concentrations of MLB under hypoxia (1% O_2,

5% CO_2) and assessed cell viability at various time points (3, 6, 12, and 24 h). At the MLB concentrations of 0, 10, 20, 40, and 80 μmol/L, no difference in the viability of HUVECs was observed at the 3 h time point; however, at the 6, 12, and 24 h time points, HUVECs viability was considerably elevated in the MLB treatment groups relative to the control group [Figure 5B]. MDA is a product of lipid peroxidation while LDH is a stable enzyme that is rapidly released into the cell culture medium following plasma membrane damage. Under hypoxia, MDA and LDH levels rose remarkably in an MLB concentration-dependent way [Figure 5C,D]. The content of GSH, an important non-enzymatic antioxidant, was decreased in HUVECs under hypoxic conditions. Similarly, a marked MLB concentration-dependent increase in GSH levels was detected in HUVECs [Figure 5E]. Furthermore, compared with the normoxic condition, the hypoxic environment contributed to a remarkable upregulation in the phosphorylation levels of NF-κB p65 (p-p65) and the proteins levels of ICAM1 in HUVECs; however, MLB treatment significantly reversed these effects in a concentration-dependent manner [Figure 5F–I]. The difference in the levels of p-IκBα or p-IKKα/β in HUVECs between the normoxia and hypoxia groups with MLB treatment was insignificant (0–80 μmol/L) [Figure 5J–L].

MLB inhibited ICAM1 expression and the adhesion of THP-1 cells by inhibiting NF-κB p65-related phosphorylation and nuclear translocation

Upon activation, NF-κB p65 would translocate to the nucleus, where it exerts its transcriptional activity. Accordingly, we detected the cellular distribution of NF-κB p65 protein in HUVECs pre- and post-treatment with 80 μmol/L MLB under hypoxia using immunofluorescence staining. Normoxia and pyrrolidinedithiocarbamate (PDTC), an inhibitor of NF-κB p65 phosphorylation, usage under hypoxia served as controls. The findings illustrated that NF-κB p65 was primarily distributed in the cytoplasm of HUVECs under normoxic conditions but was mostly concentrated in the nucleus

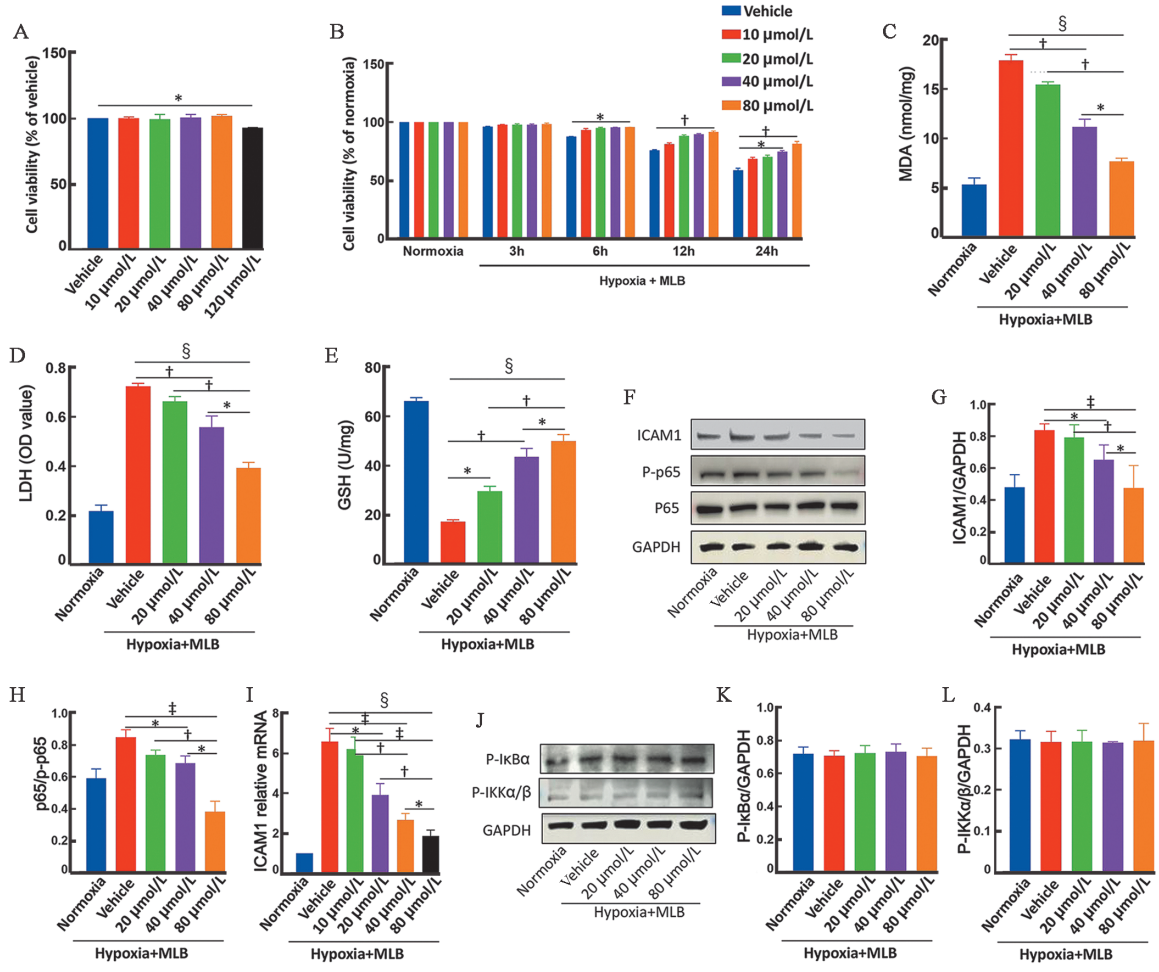

Figure 5: The impacts of MLB on the expression of NF-κB p65 and ICAM1 signaling in HUVECs. MLB enhanced the tolerance of HUVECs to hypoxic conditions. The viability of HUVECs exposed to varying concentrations of MLB for 24 h under normoxia (A) and hypoxia (B). The contents of MDA (C), LDH (D), and reduced GSH (E) were detected in HUVECs subjected to MLB for 24 h. The expression levels of ICAM1, p-p65, p65, p-IκBα, and p-IKKα/β in HUVECs treated as indicated (F–L) ($n = 3$; $^{*}P < 0.05$, $^{\dagger}P < 0.01$, $^{\ddagger}P < 0.001$, $^{\S}P < 0.0001$). GAPDH: Glyceraldehyde-3-phosphate dehydrogenase; GSH: Glutathione; HUVECs: Human umbilical vein endothelial cells; LDH: Lactate dehydrogenase; MDA: Malondialdehyde; MLB: Magnesium lithospermate B.

when the cells were cultured under hypoxia. However, when HUVECs were treated with MLB or PDTC, NF-κB p65 nuclear accumulation was significantly reduced relative to that seen with hypoxia treatment [Figure 6A]. Results of qRT-PCR and western blot illustrated that under hypoxic conditions, mRNA and protein expression levels of ICAM1, as well as NF-kappaB p65 phosphorylation levels, were considerably elevated in comparison to the normoxia group; however, these effects were noticeably reversed following treatment with MLB, PDTC, or siRNA targeting NF-κB p65 [Figure 6B–E]. Furthermore, both MLB and PDTC could significantly reduce the capacity of THP-1 cells to adhere to HUVECs under hypoxia [Figure 6F, G].

MLB attenuated hypoxia-induced ROS production and apoptosis in HUVECs

We further evaluated ROS generation and apoptosis in HUVECs under hypoxic conditions. The results proved that ROS production was increased in HUVECs cultured under hypoxia, which was reversed by MLB

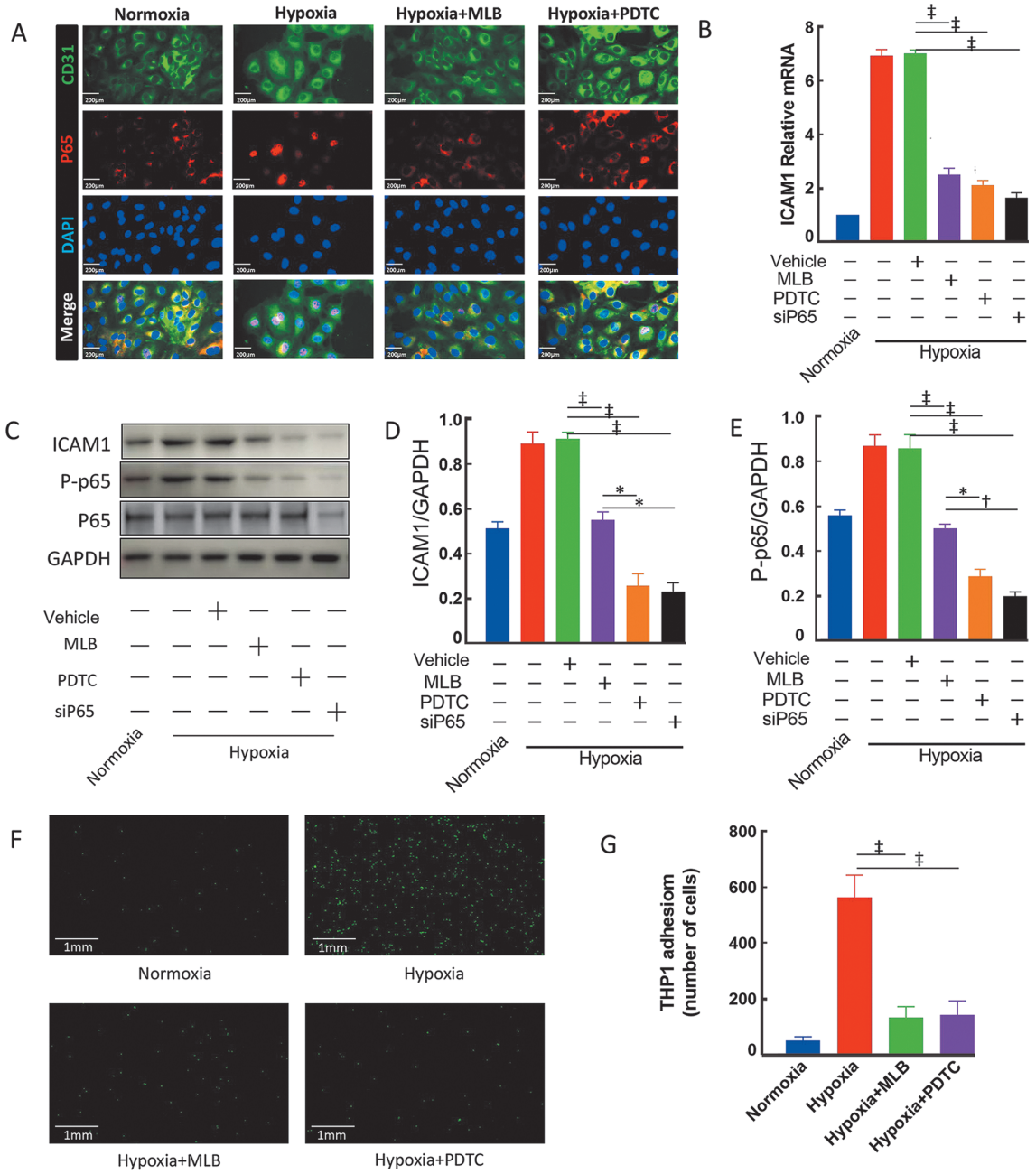

Figure 6: MLB inhibited ICAM1 expression and THP-1 cell adhesion by blocking the phosphorylation and nuclear translocation of NF-κB p65. (A) The nuclear translocation of NF-κB p65 (red) was remarkably changed in HUVECs (labeled with CD31 [green]) following treatment with MLB or PDTC under hypoxia (A). ICAM1 mRNA levels (B) and ICAM1 and p-p65 protein levels (C–E) in HUVECs were significantly decreased following treatment with MLB, PDTC, or siP65. The number of THP-1 cells that adhered to HUVECs was greatly decreased following MLB or PDTC treatment under hypoxia (F, G) ($n = 3$; $^{*}P < 0.05$, $^{\dagger}P < 0.01$, $^{\ddagger}P < 0.001$). HUVECs: Human umbilical vein endothelial cells; MLB: Magnesium lithospermate B; PDTC: Pyrrolidinedithiocarbamic acid.

treatment (80 μmol/L) [Supplementary Figure 1A, B, http://links.lww.com/CM9/B750]. In addition, TUNEL staining showed a substantial elevation in the count of TUNEL-positive HUVECs in the hypoxia treatment group in contrast with the normoxia group; however, the opposite was observed following MLB treatment (80 μmol/L) [Supplementary Figure 1C, D, http://links.lww.com/CM9/B750]. Western blot results further indicated that MLB administration reduced the levels of both BAX and cleaved-caspase-3, while remarkably increasing that of BCL2 in HUVECs [Supplementary Figure 1E, http://links.lww.com/CM9/B750].

Effects of MLB on hiPSC-CM viability and biochemical parameters under different conditions

HiPSC-CMs were cultured with various concentrations of MLB (0, 10, 20, 40, 80, and 120 μmol/L) for 24 h to investigate its effect on cell viability under normal conditions. The CCK-8 assay showed that under normal conditions, MLB concentrations of ≤40 μmol/L did not significantly affect the viability of hiPSC-CMs within 24 h, whereas at MLB concentrations of ≥80 μmol/L, hiPSC-CM viability was reduced [Supplementary Figure 2A, http://links. lww. com/CM9/B750]. To ascertain the time-dependent influence of MLB on cell viability, hiPSC-CMs were cultured under hypoxia and treated with various concentrations of MLB, and cell viability was assessed at 3, 6, 12, and 24 h after treatment. Under hypoxic conditions, the variation in hiPSC-CMs viability observed between the MLB treatment (0, 5, 10, 20, and 40 μmol/L) and control groups within 3 h was insignificant. The viability of hiPSC-CMs treated under hypoxia was inhibited after 6 h, while that of hiPSC-CMs treated with 40 μmol/L MLB showed an insignificant difference between the normoxia and hypoxia groups. Under hypoxia, the viability of hiPSC-CMs was significantly inhibited after 12 h and 24 h with all the MLB concentrations tested; however, the viability of hiPSC-CMs was substantially improved in the 40 μmol/L MLB treatment group as opposed to the blank control group [Supplementary Figure 2B, http://links.lww.com/CM9/B750]. Similar to the results obtained with the HUVECs, the contents of both MDA and LDH in the hiPSC-CMs medium increased after 24 h of hypoxia treatment; meanwhile, MLB administration led to a significant decrease in MDA and LDH contents, and these effects were dependent on the MLB dosage [Supplementary Figure 2C, D, http://links.lww.com/CM9/B750]. The GSH content was remarkably decreased in hiPSC-CMs under hypoxic conditions, and was substantially upregulated after treatment with MLB in contrast with that in the control condition in a dose-dependent manner [Supplementary Figure 2E, http://links.lww.com/CM9/B750].

MLB exerted anti-apoptotic effects in hiPSC-CMs

Under hypoxia, hiPSC-CMs were treated with varying concentrations of MLB for 24 h to examine their influence on apoptosis. Compared with the normoxia treatment, hypoxia had a significant effect on the protein expression of cleaved-caspase-3, p-STAT3, BAX, DUSP2, and BCL2 in hiPSC-CMs, while MLB treatment reversed this trend concentration-dependently [Supplementary Figure 3A–F, http://links. lww. com/CM9/B750]. The transcription factor STAT3 would translocate to the nucleus when phosphorylated and activated. Stattic is an inhibitor of STAT3 phosphorylation, which prevents STAT3 from entering the nucleus and exerting its transcriptional activity. DUSP2 is involved in apoptotic signaling mediated by the transcription factor E2F1 as well as in the regulation of STAT3 activity through dephosphorylation. The immunofluorescence staining results illustrated that, under normoxia, STAT3 was expressed in both the nucleus and cytoplasm of hiPSC-CMs, and that, under hypoxia, STAT3 was primarily found in the cytoplasm. Following MLB treatment, STAT3 was activated and then translocated to the nucleus, while the addition of stattic had a strong inhibiting impact on the above-mentioned effect [Supplementary Figure 3G, http://links.lww.com/CM9/B750]. Additionally, less than 2% of the TUNEL-positive hiPSC-CMs were observed under normoxic culture conditions, whereas approximately 20% of hiPSC-CMs exhibited TUNEL positivity after 24 h of hypoxia; with MLB treatment (40 mmol/L), this number reduced to merely 7% [Supplementary Figure 3H,I, http://links.lww.com/CM9/B750].

MLB inhibited the apoptosis of hiPSC-CMs via the DUSP2/STAT3 pathway

Using siRNAs targeting DUSP2 and STAT3, we conducted further research into the possible mechanism that might be responsible for the anti-apoptotic impact of MLB. At the 40 μmol/L concentration, MLB significantly increased the levels of p-STAT3 and the expression of BCL2 and downregulated the expression of DUSP2 and BAX; similar results were observed with siDUSP2 treatment [Supplementary Figure 4A–F, http://links.lww.com/CM9/B750]. Notably, we found that the phosphorylation of STAT3 was increased when DUSP2 expression was inhibited [Supplementary Figure 4A–C, http://links.lww.com/CM9/B750]. To explore the relationship between STAT3 activation and apoptosis in hiPSC-CMs under hypoxia, we employed siSTAT3 and stattic to respectively inhibit STAT3 expression and activation. According to the findings, exposure to stattic considerably reduced the level of STAT3 phosphorylation while having no remarkable effect on the level of protein expression. However, with siSTAT3 treatment, the expression of STAT3 and the levels of STAT3 phosphorylation (p-STAT3) were both decreased [Supplementary Figure 4G, http://links.lww.com/CM9/B750]. Notably, stattic and siSTAT3 treatment had no effect on DUSP2 expression under hypoxia [Supplementary Figure 4H, http://links.lww.com/CM9/B750], but significantly inhibited STAT3 phosphorylation and the expression levels of BCL2 both with and without MLB co-treatment [Supplementary Figure 4I, J, http://links.lww.com/CM9/B750]. Similarly, the expression levels of the apoptosis-related protein BAX were increased under hypoxia and were further significantly enhanced with stattic or siSTAT3 treatment both with and without MLB co-administration [Supplementary Figure 4K, http://links.lww.com/CM9/B750].

Discussion

Cardiomyocyte transplantation can improve cardiac function after MI *via* paracrine-induced suppression of cardiomyocyte apoptosis, promotion of angiogenesis, and functional integration.[2,3,5,7,16] Extremely high mortality of cells after transplantation is a major factor limiting ischemic heart disease-related cell therapy.[6] The survival rate of transplanted cells was reported to be lower in both ischemia–reperfusion and MI models in large part owing to the local microenvironment.[17] Moreover, studies have shown that immunosuppression can enhance the survival of transplanted cells.[18]

The inflammatory response that occurs within the first week after myocardial ischemia induces multiple impairments in cardiac microcirculation, including microvascular endothelial cell dysfunction, macromolecular efflux, ROS production, and increased leukocyte adhesion. This, in turn, exacerbates the inflammatory response, decreases coronary blood flow, and induces cardiomyocyte death,[19] in which endothelial cells play an important role. Under inflammatory conditions, macromolecules and immune cells can penetrate endothelial cells through transcellular mechanisms.[20] The expression of molecules that promote leukocyte–endothelial tip cell adhesion is often elevated in situations of acute or chronic inflammation, thereby increasing luminal leukocyte–endothelial cell interactions and, consequently, the ability of endothelial cells to capture leukocytes from the bloodstream.[21,22] ICAM1, belonging to the immunoglobulin superfamily cell adhesion molecules, is expressed in endothelial cells and plays a crucial role in mediating the migration of a variety of immune cells into the myocardium. Studies have confirmed that anti-ICAM1 monoclonal antibody treatment before ischemia–reperfusion can reduce leukocyte infiltration during myocardial ischemia–reperfusion, thereby moderating coronary vasodilation and myocardial injury.[23] Our results demonstrated that ICAM1 expression was increased in cardiac endothelial cells in a mouse model of cardiac ischemia, but was substantially reduced in cardiac endothelial cells extracted from mice that received an intraperitoneal injection of MLB after the establishment of MI. *In vitro* studies also confirmed that the expression levels of ICAM1 were increased in HUVECs cultured under hypoxia; however, this increase was suppressed by MLB treatment.

Cardiac ischemia–reperfusion induces ROS production. Meanwhile, endothelial cells, macrophages, and cardiomyocytes produce TNF-α, IL-8, IL-6, IL-1, and peptide activating factor. These processes substantially promoted neutrophil infiltration at ischemic sites, which directly accentuates the progression of cardiac infarction.[24] Adhesion molecules on the endothelium, including ICAM1, are upregulated and activate neutrophil migration through the endothelium. When neutrophils migrate to the site of ischemia–reperfusion, nicotinamide adenine dinucleotide phosphate oxidase is activated by pro-inflammatory cytokines, leading to the generation of large amounts of ROS.[25] Neutrophils were confirmed to be the most important source of ROS during ischemia by electron paramagnetic resonance spectroscopy.[26] In addition, a reduction in neutrophil infiltration was shown to be accompanied by an attenuation of myocardial necrosis in ICAM1-knockout mice in a myocardial ischemia model.[27] Even though intramyocardial injection of cells may increase local inflammation to some extent, cellular-related treatments were well known as a promising strategy in the treatment of cardiac infarction.[7,28] In the present study, using a mouse model of MI, we showed that hiPSC-CM engraftment reduced the infiltration of F4/80-positive cells, but not CD11b-positive cells, which may have resulted from the paracrine effect of the transplanted hiPSC-CMs. However, the addition of MLB inhibited the infiltration of both CD11b-positive and F4/80-positive cells during MI [Figure 4D–G]. This may be due in part to the fact that MLB treatment reduced ICAM1 expression in myocardial endothelial cells, thus diminishing inflammatory cell infiltration and improving cardiac function after ischemia. *In vitro* experiments further showed that MLB treatment can significantly reduce the adhesive capacity of THP-1 cells to HUVECs.

NF-κB is a transcriptional factor that performs a fundamental function in regulating tissue inflammation, oxidative stress, and cell death.[29] In the resting state, the p50/p65 heterodimer (the primary form of NF-κB found in endothelial cells) is sequestered in the cytoplasm *via* its association with the IκBα.[30] Once cells are stimulated by pro-inflammatory factors, IκBα is phosphorylated by the IKK complex, which consists of two catalytically active kinases, IKKα and IKKβ, and a regulatory subunit, IKKγ.[31] The phosphorylation of IκBα induces its ubiquitination and proteasome-dependent degradation, facilitating the release of active dimeric NF-κB, which subsequently localizes to the nucleus and triggers the transcription of downstream genes such as *ICAM1*.[32] Under hypoxia, we discovered that MLB suppressed NF-kB p activation by specifically suppressing p65 phosphorylation of NF-κB independent of IκBα and IKKα/β phosphorylation [Figure 5J–L]. The protein and mRNA expression of ICAM1 was downregulated when NF-κB p65 was knocked down, which further demonstrated that the MLB-mediated decrease in ICAM1 protein expression was partially achieved through the inhibition of NF-κB p65 phosphorylation [Supplementary Figure 5, http://links.lww.com/CM9/B750].

ROS are important inducers of apoptosis and associated signaling pathways. Research demonstrates that ROS are the main trigger of apoptosis in cardiac disease, while antioxidant treatment remarkably reduces myocardial apoptosis after ischemia.[33] Additionally, the culturing of cardiomyocytes in an exogenous ROS-generating system have resulted in cytochrome release and the activation of caspase-3.[33] Activated neutrophils and macrophages might generate ROS, which has a role in both the onset and progression of apoptosis.[34] We discovered that, under hypoxia, ROS levels were increased in HUVECs, whereas the addition of MLB reduced ROS production and the rate of cell apoptosis in these cells [Supplementary Figure 1, http://links.lww.com/CM9/B750].

One reason underlying the poor survival of transplanted cells post-MI is the presence of a hypoxic microenvironment, which accelerates cell death. Existing literature demonstrates that hiPSC-CM apoptosis can be reduced and the survival of transplanted cells can be increased by inhibiting the activity of Rho kinase.[35] Herein, we discovered that the viability of hiPSC-CMs was remarkably decreased under hypoxic conditions; however, the addition of MLB greatly improved the viability of hiPSC-CMs and significantly reduced the LDH content in the cell culture medium [Supplementary Figure 2B, C, http://links.lww.com/CM9/B750]. LDH activity is commonly used as a measure of myocardial cell damage. When the cell membrane is damaged, intracellular LDH can leak out into the extracellular fluid. Meanwhile, under hypoxic conditions, lipid peroxidation markers such as MDA levels rose remarkably [Supplementary Figure 2D and Figure 5, http://links.lww.com/CM9/B750]; however, MLB treatment reduced hypoxia-induced lipid peroxidation-related damage in hiPSC-CMs. Members of the BCL2 family of proteins are key regulators of cardiomyocyte apoptosis[36] and can be divided into two main categories according to their functions, namely, pro-apoptotic and anti-apoptotic.[6,37] BCL2 is the most important anti-apoptotic marker, while BAX is the primary pro-apoptotic marker, both of which perform instrumental functions in regulating apoptosis. The BAX/BCL2 ratio is a key determinant of cell death or survival. An increase in BCL2 protein expression in cells promotes the separation of BAX homodimers, thus allowing BCL2 to bind to monomeric BAX, resulting in the formation of a more stable BAX/BCL2 heterodimer complex that favors cell survival. In contrast, when the BAX/BAX dimer content is high, apoptosis is promoted. Numerous studies have confirmed that BAX dimerization and, consequently, cell apoptosis are significantly increased when cardiomyocytes are cultured in a hypoxic environment. Herein, we found that when MLB was added to hiPSC-CMs cultured in a hypoxic environment, the BCL2 levels were significantly upregulated, whereas those of BAX were significantly downregulated. TUNEL staining confirmed that the rate of apoptosis among hiPSC-CMs decreased with MLB administration. To further confirm that MLB can increase the number of hiPSC-CMs that successfully engraft *in vivo*, we established a mouse model of MI, and then injected hiPSC-CMs into the infarct site, followed by the intraperitoneal injection of MLB. We found that the survival rate of the administered hiPSC-CMs was significantly improved with MLB administration, as was the cardiac function of the mice.

Research has demonstrated that the JAK/STAT pathway is activated during ischemic injury, resulting in the modulation of the biological activity of downstream substrate molecules through phosphorylation.[38] STAT3 has a key cardioprotective role.[39] Additionally, the JAK2/STAT3 signaling pathway was reported to participate in the anti-apoptotic effect of ischemic preconditioning by promoting the synthesis of BCL2 and inhibiting that of BAX.[40] In this study, we found that STAT3 phosphorylation was inhibited in hiPSC-CMs after hypoxia treatment; however, the addition of MLB could effectively block this effect, thereby inhibiting the expression of downstream pro-apoptotic genes. The expression of DUSP2, a key STAT3 phosphatase,[41] was significantly upregulated in hypoxia-treated hiPSC-CMs. Here, we found that MLB exerted its cardioprotective effect mainly by reducing the expression of DUSP2 and, consequently, the dephosphorylation of STAT3 [Supplementary Figure 4A,5, http://links.lww.com/CM9/B750].

Our observations are limited by the study's duration (1 month), which precluded us from examining the long-term fate of the transplanted cells. Thus, future investigations are needed to comprehensively characterize the mechanisms through which MLB and hiPSC-CMs administration improves myocardial recovery from MI. Additionally, it is imperative to assess the long-term safety and effectiveness of this treatment. In conclusion, we demonstrated that MLB can suppress the ICAM1 levels in cardiac endothelial cells of mice following MI as well as reduce the numbers of lymphocytes and macrophages at the site of MI. MLB significantly improved endothelial cell function *via* the NF-κB/ICAM1 pathway. We further showed that MLB can reduce the levels of apoptosis of hiPSC-CMs cultured in a hypoxic environment through the DUSP2/STAT3 pathway [Supplementary Figure 5, http://links.lww.com/CM9/B750]. Accordingly, MLB effectively improved the survival rate of transplanted hiPSC-CMs as well as the cardiac function of mice after MI. To achieve the ultimate clinical objective of MI therapy in patients, further studies should consider investigating the fully mechanism of MLB on hiPSC-CMs in MI heart with large animal models. The present strategy provides a potential application prospect for the combination of Chinese traditional herbal monomer and cell therapy in the treatment of MI.

Funding

This work was financially supported by the Natural Science Foundation of Hunan Province (Nos. 2023JJ30793, 2022JJ20088, and 2019JJ50858), the Science and Technology Innovation Program of Hunan Province (No. 2021RC2106), the National Natural Science Foundation of China (No. 82200323), and the Scientific Research Launch Project for new employees of the Second Xiangya Hospital of Central South University.

Conflicts of interest

CF is a postdoctoral researcher from Hunan Fangsheng Pharmaceutical Co., Ltd. JG worked for Hunan Fangsheng Pharmaceutical Co., Ltd.

References

1. Tsao CW, Aday AW, Almarzooq ZI, Alonso A, Beaton AZ, Bittencourt MS, *et al*. Heart disease and stroke statistics-2022 update: A report from the American Heart Association. Circulation 2022;145:e153–e639. doi: 10.1161/CIR.0000000000001052.
2. Fan C, Tang Y, Zhao M, Lou X, Pretorius D, Menasche P, *et al*. CHIR99021 and fibroblast growth factor 1 enhance the regenerative potency of human cardiac muscle patch after myocardial infarction in mice. J Mol Cell Cardiol 2020;141:1–10. doi: 10.1016/j.yjmcc.2020.03.003.
3. Fan C, Fast VG, Tang Y, Zhao M, Turner JF, Krishnamurthy P, *et al*. Cardiomyocytes from CCND2-overexpressing human induced-

pluripotent stem cells repopulate the myocardial scar in mice: A 6-month study. J Mol Cell Cardiol 2019;137:25–33. doi: 10.1016/j.yjmcc.2019.09.011.
4. Fan C, Oduk Y, Zhao M, Lou X, Tang Y, Pretorius D, *et al*. Myocardial protection by nanomaterials formulated with CHIR99021 and FGF1. JCI Insight 2020;5:e132796. doi: 10.1172/jci.insight.132796.
5. Wu X, Wang D, Qin K, Iroegbu CD, Xiang K, Zhou Y, *et al*. Cardiac repair with echocardiography-guided multiple percutaneous left ventricular intramyocardial injection of hiPSC-CMs after myocardial infarction. Front Cardiovasc Med 2021;8:768873. doi: 10.3389/fcvm.2021.768873.
6. Wu X, Iroegbu CD, Peng J, Guo J, Yang J, Fan C. Cell death and exosomes regulation after myocardial infarction and ischemia-reperfusion. Front Cell Dev Biol 2021;9:673677. doi: 10.3389/fcell.2021.673677.
7. Tang S, Fan C, Iroegbu CD, Zhou W, Zhang Z, Wu M, *et al*. TMSB4 overexpression enhances the potency of marrow mesenchymal stromal cells for myocardial repair. Front Cell Dev Biol 2021;9:670913. doi: 10.3389/fcell.2021.670913.
8. Yellon DM, Hausenloy DJ. Myocardial reperfusion injury. N Engl J Med 2007;357:1121–1135. doi: 10.1056/NEJMra071667.
9. Frangogiannis NG. Regulation of the inflammatory response in cardiac repair. Circ Res 2012;110:159–173. doi: 10.1161/CIRCRESAHA.111.243162.
10. Li ZM, Xu SW, Liu PQ. Salvia miltiorrhizaBurge (Danshen): A golden herbal medicine in cardiovascular therapeutics. Acta Pharmacol Sin 2018;39:802–824. doi: 10.1038/aps.2017.193.
11. Wang J, Xiong X, Feng B. Cardiovascular effects of salvianolic acid B. Evid Based Complement Alternat Med 2013;2013:247948. doi: 10.1155/2013/247948.
12. Luo X, Deng Q, Xue Y, Zhang T, Wu Z, Peng H, *et al*. Antifibrosis effects of magnesium lithospermate B in experimental pulmonary fibrosis: By inhibiting TGF-betaRI/Smad signaling. Molecules 2021;26:1715. doi: 10.3390/molecules26061715.
13. Paik YH, Yoon YJ, Lee HC, Jung MK, Kang SH, Chung SI, *et al*. Antifibrotic effects of magnesium lithospermate B on hepatic stellate cells and thioacetamide-induced cirrhotic rats. Exp Mol Med 2011;43:341–349. doi: 10.3858/emm.2011.43.6.037.
14. Hur KY, Seo HJ, Kang ES, Kim SH, Song S, Kim EH, *et al*. Therapeutic effect of magnesium lithospermate B on neointimal formation after balloon-induced vascular injury. Eur J Pharmacol 2008;586:226–233. doi: 10.1016/j.ejphar.2008.02.072.
15. Tai Y, Qiu Y, Bao Z. Magnesium lithospermate B suppresses lipopolysaccharide-induced neuroinflammation in BV2 microglial cells and attenuates neurodegeneration in lipopolysaccharide-injected mice. J Mol Neurosci 2018;64:80–92. doi: 10.1007/s12031-017-1007-9.
16. Shiba Y, Gomibuchi T, Seto T, Wada Y, Ichimura H, Tanaka Y, *et al*. Allogeneic transplantation of iPS cell-derived cardiomyocytes regenerates primate hearts. Nature 2016;538:388–391. doi: 10.1038/nature19815.
17. Yu Y, Qin N, Lu XA, Li J, Han X, Ni X, *et al*. Human embryonic stem cell-derived cardiomyocyte therapy in mouse permanent ischemia and ischemia-reperfusion models. Stem Cell Res Ther 2019;10:167. doi: 10.1186/s13287-019-1271-4.
18. Pearl JI, Lee AS, Leveson-Gower DB, Sun N, Ghosh Z, Lan F, *et al*. Short-term immunosuppression promotes engraftment of embryonic and induced pluripotent stem cells. Cell Stem Cell 2011;8:309–317. doi: 10.1016/j.stem.2011.01.012.
19. Zhao N, Liu YY, Wang F, Hu BH, Sun K, Chang X, *et al*. Cardiotonic pills, a compound Chinese medicine, protects ischemia-reperfusion-induced microcirculatory disturbance and myocardial damage in rats. Am J Physiol Heart Circ Physiol 2010;298:H1166–H1176. doi: 10.1152/ajpheart.01186.2009.
20. Amersfoort J, Eelen G, Carmeliet P. Immunomodulation by endothelial cells – Partnering up with the immune system? Nat Rev Immunol 2022;22:576–588. doi: 10.1038/s41577-022-00694-4.
21. Reglero-Real N, Marcos-Ramiro B, Millán J. Endothelial membrane reorganization during leukocyte extravasation. Cell Mol Life Sci 2012;69:3079–3099. doi: 10.1007/s00018-012-0987-4.
22. Ley K, Laudanna C, Cybulsky MI, Nourshargh S. Getting to the site of inflammation: The leukocyte adhesion cascade updated. Nat Rev Immunol 2007;7:678–689. doi: 10.1038/nri2156.
23. Ma XL, Lefer DJ, Lefer AM, Rothlein R. Coronary endothelial and cardiac protective effects of a monoclonal antibody to intercellular adhesion molecule-1 in myocardial ischemia and reperfusion. Circulation 1992;86:937–946. doi: 10.1161/01.cir.86.3.937.
24. Ma Y. Role of neutrophils in cardiac injury and repair following myocardial infarction. Cells 2021;10:1676. doi: 10.3390/cells10071676.
25. El-Benna J, Dang PM, Gougerot-Pocidalo MA. Priming of the neutrophil NADPH oxidase activation: Role of p47phox phosphorylation and NOX2 mobilization to the plasma membrane. Semin Immunopathol 2008;30:279–289. doi: 10.1007/s00281-008-0118-3.
26. Duilio C, Ambrosio G, Kuppusamy P, DiPaula A, Becker LC, Zweier JL. Neutrophils are primary source of O_2 radicals during reperfusion after prolonged myocardial ischemia. Am J Physiol Heart Circ Physiol 2001;280:H2649–H2657. doi: 10.1152/ajpheart.2001.280.6.H2649.
27. Starz C, Härdtner C, Mauler M, Dufner B, Hoppe N, Krebs K, *et al*. Elevated platelet-leukocyte complexes are associated with, but dispensable for myocardial ischemia-reperfusion injury. Basic Res Cardiol 2022;117:61. doi: 10.1007/s00395-022-00970-3.
28. Shao L, Shen Y, Ren C, Kobayashi S, Asahara T, Yang J. Inflammation in myocardial infarction: Roles of mesenchymal stem cells and their secretome. Cell Death Discov 2022;8:452. doi: 10.1038/s41420-022-01235-7.
29. Cheng W, Cui C, Liu G, Ye C, Shao F, Bagchi AK, *et al*. NF-kappaB, a potential therapeutic target in cardiovascular diseases. Cardiovasc Drugs Ther 2023;37:571–584. doi: 10.1007/s10557-022-07362-8.
30. Chen ZJ, Parent L, Maniatis T. Site-specific phosphorylation of IkappaBalpha by a novel ubiquitination-dependent protein kinase activity. Cell 1996;84:853–862. doi: 10.1016/s0092-8674(00)81064-8.
31. Lenardo MJ, Fan CM, Maniatis T, Baltimore D. The involvement of NF-kappa B in beta-interferon gene regulation reveals its role as widely inducible mediator of signal transduction. Cell 1989;57:287–294. doi: 10.1016/0092-8674(89)90966-5.
32. Zhong Y, He S, Huang K, Liang M. Neferine suppresses vascular endothelial inflammation by inhibiting the NF-kappaB signaling pathway. Arch Biochem Biophys 2020;696:108595. doi: 10.1016/j.abb.2020.108595.
33. Mongirdienė A, Skrodenis L, Varoneckaitė L, Varoneckaitė G, Gerulis J. Reactive oxygen species induced pathways in heart failure pathogenesis and potential therapeutic strategies. Biomedicines 2022;10:602. doi: 10.3390/biomedicines10030602.
34. Morris G, Gevezova M, Sarafian V, Maes M. Redox regulation of the immune response. Cell Mol Immunol 2022;19:1079–1101. doi: 10.1038/s41423-022-00902-0.
35. Zhao M, Tang Y, Ernst PJ, Kahn-Krell A, Fan C, Pretorius D, *et al*. Enhancing the engraftment of human induced pluripotent stem cell-derived cardiomyocytes via a transient inhibition of Rho kinase activity. J Vis Exp 2019;149. doi: 10.3791/59452.
36. Korshunova AY, Blagonravov ML, Neborak EV, Syatkin SP, Sklifasovskaya AP, Semyatov SM, *et al*. BCL2-regulated apoptotic process in myocardial ischemia-reperfusion injury (Review). Int J Mol Med 2021;47:23–36. doi: 10.3892/ijmm.2020.4781.
37. Wu X, Qin K, Iroegbu CD, Xiang K, Peng J, Guo J, *et al*. Genetic analysis of potential biomarkers and therapeutic targets in ferroptosis from coronary artery disease. J Cell Mol Med 2022;26:2177–2190. doi: 10.1111/jcmm.17239.
38. Boengler K, Hilfiker-Kleiner D, Drexler H, Heusch G, Schulz R. The myocardial JAK/STAT pathway: From protection to failure. Pharmacol Ther 2008;120:172–185. doi: 10.1016/j.pharmthera.2008.08.002.
39. Bolli R, Stein AB, Guo Y, Wang OL, Rokosh G, Dawn B, *et al*. A murine model of inducible, cardiac-specific deletion of STAT3: Its use to determine the role of STAT3 in the upregulation of cardioprotective proteins by ischemic preconditioning. J Mol Cell Cardiol 2011;50:589–597. doi: 10.1016/j.yjmcc.2011.01.002.
40. Hattori R, Maulik N, Otani H, Zhu L, Cordis G, Engelman RM, *et al*. Role of STAT3 in ischemic preconditioning. J Mol Cell Cardiol 2001;33:1929–1936. doi: 10.1006/jmcc.2001.1456.
41. Kanemaru H, Yamane F, Tanaka H, Maeda K, Satoh T, Akira S. BATF2 activates DUSP2 gene expression and up-regulates NF-kappaB activity via phospho-STAT3 dephosphorylation. Int Immunol 2018;30:255–265. doi: 10.1093/intimm/dxy023.

How to cite this article: Fan CM, Qin KL, Iroegbu CD, Xiang K, Gong YB, Guan Q, Wang WX, Peng J, Guo JJ, Wu X, Yang JF. Magnesium lithospermate B enhances the potential of human-induced pluripotent stem cell-derived cardiomyocytes for myocardial repair. Chin Med J 2024;137:1857–1869. doi: 10.1097/CM9.0000000000002867